J Math Chem (2009) 46:576–585
DOI 10.1007/s10910-008-9483-3

ORIGINAL PAPER

Exploration for electronic transitions and photodissociation mechanism of hydrogen iodide

Dongfang Zhang

Received: 23 August 2008 / Accepted: 6 October 2008 / Published online: 21 November 2008

Abstract The electronic transitions and excited-state fragmentation of hydrogen iodide have been studied within the A-band continuum. The extinction intensity for the excitations from the ground to the low-lying electronic states are derived by performing the wave packet simulations of nuclear dynamics in this study. The quantum yields of the spin-excited $I^*(^2P_{1/2})$ product at the different photon energies are determined as well. The results suggest that the possibility of intersystem crossing can be neglected. Employing the time-dependent density functional theory (TDDFT), the four highest occupied and the two lowest unoccupied orbitals of hydrogen iodide have been analyzed, and the transition to the $A^1\Pi_1$ state is found to be most probable in the first absorption band.

Keywords Electronic transition · Quantum yield · Photodissociation

1 Introduction

Over the last few decades, the quantum wave packet has been developed into an indispensable concept in the study of elementary molecular and chemical process. Putting particle dynamics under the framework of quantum mechanics it will facilitate our understanding of the wave properties of matter. A notable example of this dual nature is molecular wave packet interference at conical intersections of potential energy surfaces which, to the utmost, may close otherwise available propagation routes [1–4]. Obviously, such dynamical restrictions on the available molecular phase space could strictly modify the course of chemical reactions which inspires continued investigation of consequences of quantum wave packet interference in molecules.

D. Zhang (✉)
College of Science, Huazhong Agricultural University, Wuhan 430070, People's Republic of China
e-mail: zdfbubai@yahoo.com

The fragmentation of diatomic halogen molecules following excitation in the first absorption profile has long been a source of fascination to researchers, and they serve as benchmark systems to study the electronic transition and the spectroscopy. Recent experimental activities have been devoted to the study of the orientation and alignment, namely the m_j distributions of the product angular momentum. Details of the nonadiabatic transition probabilities have been estimated from such analysis for molecular chlorine [5–7]. Classical investigations of the discrete absorption spectra have resulted in the accurate identification of transitions between specific vibrational and rotational levels of these diatomics. Also, recent advances in both experimental and theoretical studies of multi-channel photodisociation of small molecules [8–19] enable us to investigate quite detailed information on the dissociation dynamics. Such analyses have permitted the precise characterization of the potential curves for the electronic ground and excited states. A drawback, common to the above methods, is that such techniques cannot, however, to be used for the study of repulsive states or those portions of bound excited states which lie above the thermochemical threshold for dissociation into open-shell atomic fragments in ground configuration with which they correlate.

The present work investigates theoretically spectroscopic transitions and introduces the simulation techniques to reproduce comparable with experiment spectroscopic properties in the hydrogen iodide. Electronic structure calculations are performed to determine potential curves of various electronic states. Absorption spectra are calculated employing time-dependent propagation methods. The central result is the prediction of the wavelength dependence of the relative quantum yields of the $H + I^*$ channel on laser wavelength, which provides an insight into the nature of the electronic excited states that participate in the photodissociation and in good quantitative agreement with experiment. The time-dependent density functional theory (TDDFT) is applied to study the electronic transitions and molecular orbital to further illustrate the dissociation process.

2 Numerical methods

The numerical methods needed to deal with the photofragmentation involve solution of the radial Schrödinger equation

$$i\hbar\frac{\partial\Phi(r,t)}{\partial t} = \hat{H}(r)\Phi(r,t) = \left[-\frac{\hbar^2}{2\mu}\cdot\frac{d^2}{dr^2} + \hat{V}(r)\right]\Phi(r,t) \tag{1}$$

where r is the nuclear coordinate, μ the reduced mass of hydrogen iodide, V(r) the adiabatic potential energy and Φ(r, t) is the time-dependent wave function.

The initial wave packets Φ_n(r, t) are created by means of the ground state vibrational wave function Ψ(r) times the appropriate transition dipole functions

$$\Phi_n(r, t = 0) = M_n(r)\Psi(r) \tag{2}$$

$\Phi_n(r, t=0)$ in Eq. 2 denotes the wave packet associated with the nth excited state and $M_n(r)$ is the associated transition moment.

Wave packet propagation is accomplished using the split operator (time step is *dt* scheme

$$\Phi(r, t+dt) = e^{-i\widehat{T}dt/2\hbar} e^{-i\widehat{V}dt/\hbar} e^{-i\widehat{T}dt/2\hbar} \times \Phi(r, t) \tag{3}$$

The dynamics is probed at an analysis line fixed at a large value of $r = r_\infty$. Energy dependent amplitudes B_n (r_∞, E) are obtained by Fourier transformation [20]

$$B_n(r_\infty, E) = \frac{1}{2\pi} \int_0^\infty \Phi_n(r_\infty, t) \exp[i(E_0 + h\nu)t/\hbar] dt \tag{4}$$

where E_0 is the energy of origin transition, $h\nu$ denotes the incident energy. The partial cross sections are obtained by

$$\sigma_n(\nu) = \frac{32\pi\nu k_n}{3c\varepsilon_0} |B_n(r_\infty, E)|^2 \tag{5}$$

where k_n is the asymptotic wave vector for the nth channel. The total cross section amounts to the sum of the partial cross section,

$$\sigma_{tot}(\nu) = \sum_{n=1}^{4} F_n \sigma_n(\nu) \tag{6}$$

where F_n is a degeneracy factor of the upper dissociative state, which equals to 2, 2, 1 and 2 for $a^3\Pi_1$, $A^1\Pi_1$, $a^3\Pi_0{}^+$ and $t^3\Sigma_1{}^+$ states, respectively.

In order to get rid of the spurious recurrences at the small r and the upper end of the grid, the wave functions must be dissipated when they reach the asymptotic region of the grid. The intensity of absorbing potential are defined by

$$S_{abs}(r) = 1.0 \quad r < r_{abs} \tag{7}$$

$$S_{abs}(r) = \exp(-S_{opt} \cdot dt) \left(\frac{r - r_{abs}}{r_{max} - r_{abs}} \right)^{3/2} \quad r_{abs} < r < r_{max} \tag{8}$$

where r_{abs} is the incipient point of damping and S_{opt} is an optimum factor to modulate damping force. Values of all parameters used in calculations are listed in Table 1. The ground state and low-lying excited states of hydrogen iodide are derived by using the casscf procedure in the molcas 5.4 computer codes [21]. In the calculations, the relevant eight electrons are set as active, and the orbital inspection are carried out by RHF/STO-3G method. Practical active spaces increase to about six orbital for energies and gradients, which involve σ_{HI}, σ^*_{HI}, $\pi 5p_x$, $\pi 5p_y$ and two nonvalence virtual orbitals. The basis set of double quality (cc-pVDZ) is used for hydrogen and the ab initio model potential (AIMP) [22] is used for iodine. The associated valence basis functions of (3s, 3p) were used without contraction and augmented by a set of diffuse s and p orbitals

Table 1 The input parameters to perform the time-dependent wave packet calculation

Variable	Description	Value
Atomic masses	μ_H	1.0079 amu
	μ_I	126.9045 amu
Reduced masses	μ	1823.02 a.u.
Range of grid	r_{min}, r_{max}	2.363–14.952 a_0
Number of grid points		2048
Position of r_∞		9.452 a_0
Time step	dt	0.483776 fs
Number of time steps		8192
Start of absorbing region	r_{abs}	9.952 a_0
Damping coefficient	S_{opt}	0.015 fs^{-1}

($\alpha_s = 0.0395$, $\alpha_p = 0.0432$), and two sets of d ($\alpha_d = 0.3596$ and 0.1785), a set of f ($\alpha_f = 0.33$) and a set of g ($\alpha_g = 0.427$) functions. The basis sets are thus expressed as (4s, 4p, 2d, 1f, 1g).

3 Results and discussion

The calculated adiabatic potential curves of HI system are shown in Fig. 1. Restricted by the electric-dipole-forbidden and selection rules, the pertinent excited state potential curves that initially populated in the near ultraviolet region of the spectrum are four Ω states, as displayed in the graph. These states are marked by $a^3\Pi_0{}^+$ (non degenerate) and $a^3\Pi_1$, $t^3\Sigma_1{}^+$, $A^1\Pi_1$ (all comprising two substates). The presence of iodine element brings a large spin–excited interaction ($E_{so} = 0.943$ eV), so a more suitable coupling case should occur at the atomic level. However, the customary notation to describe the state is followed, with its Ω component and multiplicity. In an equilibrium geometry of nucleus, the potential curves of the state $A^1\Pi_1$, are associated with the ground $X^1\Sigma_{0+}{}^+$ curve by the allowed transitions, i.e., $\Delta\Omega = \pm 1$ (perpendicular character), which consists of the adiabatic dissociation path to the production of atomic I. In contrast, the $a^3\Pi_0^+$ state, which will be responsible for the direct photodissociation channel of $H + I^*$, are attained by a parallel type excitation ($\Delta\Omega = 0$) : $a^3\Pi_0{}^+ \leftarrow X$. In the present calculations, the spin–orbit effect acts as a coupling between diabatic states. The available information on the associated transition dipole matrix, the permanent dipole moments, and the spin–orbit coupling curves was obtained from Ref. [23]. The equilibrium bond length of $X^1\Sigma_0{}^+$ state is calculated to be 3.051 bohr and agrees with experimental data [24] of 3.041 bohr. The dissociation energy, calculated from the $X^1\Sigma_0{}^+$ state at its equilibrium internuclear distance is 3.372 eV and compares well to the experimental value [24] of 3.196 eV with the difference being 2.4%. Fitting the low-lying vibrational states of HI to a simple anharmonic oscillator expression and determine the energies by utilizing the Fourier grid Hamiltonian method [25], the obtained harmonic frequency, $\omega_e = 2357.62\ cm^{-1}$ are in line with the experimental values [24] of 2309 cm^{-1}. In addition, the magnitude of the vertical excitation energies of the present work for the excitation from the X state to the $a^3\Pi_1$, $a^3\Pi_0{}^+$ and $A^1\Pi_1$

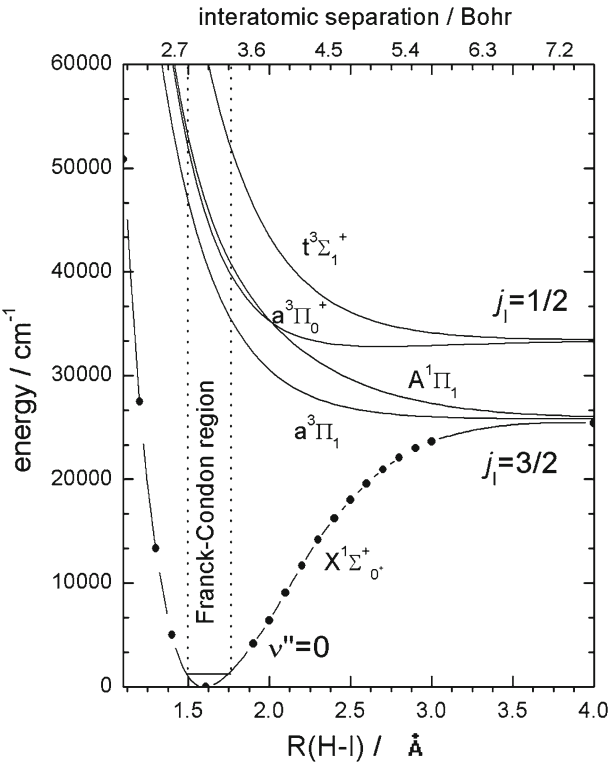

Fig. 1 The potential energy curves for low-lying states of hydrogen iodide

electronic states are 40693, 44741 and 47296 cm^{-1}, which are in agreement with the former measurements [24]. The close agreement of these calculated properties of the potential energy curves with the corresponding experimental quantities is evidence of this method's accuracy.

In the light of the theoretical value of the position of the RKR turning points for ground $\nu'' = 0$ level, the Franck-Condon overlap region is drawn, the boundaries of which (1.49–1.76 Å) are represented by vertical dotted lines. It is found that the two states ($a^3\Pi_0{}^+$ and $A^1\Pi_1$) cross each other within the propagation paths of wave packet, which coordinate lies outside the Franck-Condon excitation zone due to these two states are distinct from each other on the energy scale. Since the flux separate at the place somewhat far away from the final stage of the dissociation, the recoil distribution of product might be less anisotropic if the component mixing with different angular momentum takes place. Although in HI all optically allowed transitions can contribute, however, the direct $t^3\Sigma_1{}^+ \leftarrow X$ transition contributes only at high energy because of the relative positions of the potential energy curves. Thus the initial excitation relevant to discussion should be limited to the three optically accessible excited states, that is, the $A^1\Pi_1$, $a^3\Pi_1$ and $a^3\Pi_0{}^+$ electronic states.

To determine the extinction intensity for the photodissociation of HI molecule, the numerical methods mentioned above are utilized. The transition mechanism is

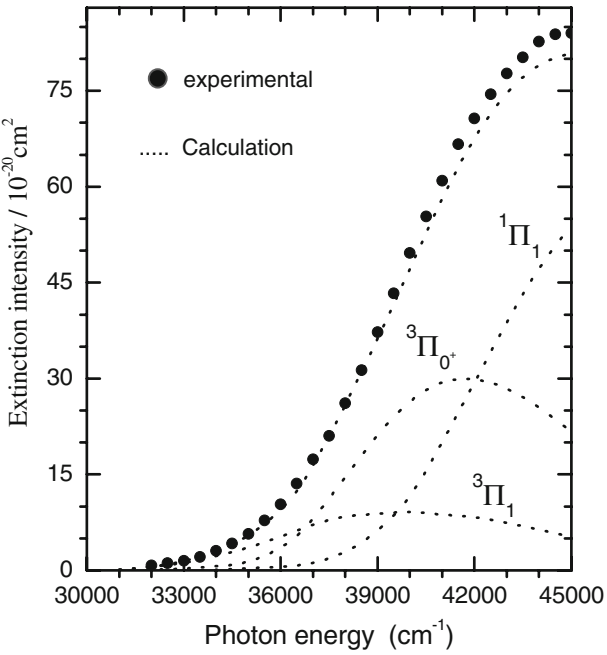

Fig. 2 Intensity profile of the partial and total absorption spectrum for a part of the A band: *dotted line*, calculated value; •, experimental data

assumed to involve a single photon absorption that causes the molecule transfer to a dissociative electronic surface. The results of the extinction intensity that associated with the electronic transitions to the $A^1\Pi_1$, $a^3\Pi_1$ and $a^3\Pi_0{}^+$ states are given in Fig. 2, also shown is the total extinction intensity, which corresponds to the sum of each partial extinction intensity. With the purpose of comparison, gas-phase absorption spectrum of HI recorded at 298 K (symbol •) by Ogilvie et al. [26] is given in the graph. It can be seen that the overall shape of the absorption spectrum is featureless with broad envelopes. Although it is in good accord with that actually observed with the path length employed, there are slight deviations in the magnitude of total extinction intensity near the intermediate region of this A spectrum band. For instance, the extinction intensity is calculated to be $\sigma = 8.098 \times 10^{-19}\text{cm}^2$ at 45000cm^{-1}, the corresponding measured value is $8.27 \times 10^{-19}\text{cm}^2$. It also can note the defects become visible from the beginning about $42000\,\text{cm}^{-1}$, particularly in the range of $43000–45000\,\text{cm}^{-1}$, in which a considerable part of the optical extinction is rightly dominated by the occurrence of $A^1\Pi_1 \leftarrow X$ transition. The overall spectrum in foregoing region still varies smoothly, so the calculated values lying systematically lower by about 3%, but it is small to be within the uncertainty (±5%) for one standard deviation in terms of the accuracy of the pressure measurements that employed [26].

The normal checks for exploring the photodissociation channels that correlate to the low lying excited states of HI have been carried out and the relevant molecular orbitals have been examined. Fig. 3 shows the four highest occupied molecular orbitals

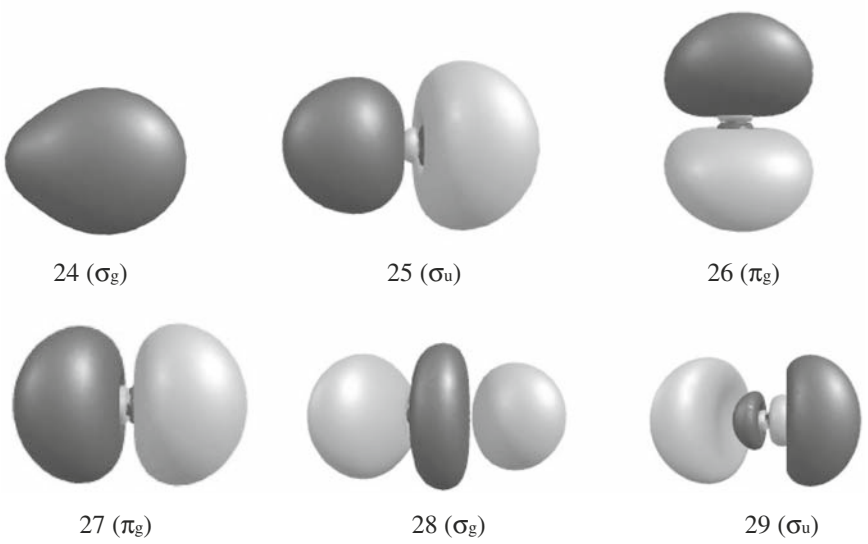

Fig. 3 The four highest occupied and the two lowest unoccupied orbital of HI predicted at TD-B3pw91/dgdzvp level

Table 2 Compilation of the results of HI for the transitions from the ground state to the low-lying excited states

Main excitation	Transition energies ΔE (eV)	Excitation wavelength (nm)	Coefficients of components	Oscillator strengths
25 → 28	4.986	248.66	0.7340	f = 0.0000
26 → 28	5.519	224.65	0.6805	f = 0.0000
27 → 28	5.862	211.50	0.7744	f = 0.0021
24 → 29	10.701	115.86	0.6070	f = 0.4671

(HOMO) and the two lowest unoccupied orbitals (LUMO) with their related bonding nature, which are computed at the TD-B3pw91/dgdzvp level. For the convenience of marking the π orbital, the halogen–halogen bond direction is defined as Z-axis. Clearly in the picture, the p lone-pair orbitals of the iodine atoms, which are the four energetically highest occupied MOs, constitute the main source for the formation of the low-lying excited states. Table 2 summarizes the low-lying excitations of the parent HI molecule.

According to the TD-DFT computations, the energy required for transition (24 → 29) from HOMO (H-4) to LUMO (L+2) is calculated to be 10.701 eV, and this transition seems to dominate the absorption regarding the magnitude of oscillator strength. However, the excitation energy for the 24 → 29 transition lies very close to the Rydberg transition. Thus the A-band spectrum band should be ascribed mainly to the transitions to the first lowest unoccupied molecular orbital, i.e., the front virtual orbital (L + 1). The orbital energy obtained for the highest occupied molecular orbital (H-1) is −0.2497 hartree, while the front LUMO (L + 1) has orbital energy of −0.0343

hartree. Therefore, the photon energy required for excitation is about 5.862 eV and transition to $A^1\Pi_1$ state can be achieved. This indicates that the absorption profile will show a maximum value near the wavelength of 211.5 nm, which accords with the experimental results of ~222 nm [26].

The quantum yield for product channel H + I* after optical absorption from the X state has been estimated in the present work, which is expressed in the adiabatic approximation as

$$\Phi(H + I^*) = \frac{\sigma[H + I^*]}{\sigma[H + I^*] + \sigma[H + I]} = \frac{\sigma[^3\Pi_{0^+}]}{\sigma[Total]} \tag{9}$$

where σ[H + I*] and σ[H + I] are, respectively, the extinction intensities of H + I* and H + I channels following dissociation. In this case, it means the relative fraction of total absorption σ[Total] leading to the population on the $^3\Pi_{0+}$ state, i.e., $\sigma[^3\Pi_0{}^+]$ at each wavelength. The experimental data [13–20] of quantum yield Φ for H + I* channel are depicted in Fig. 4, which are compared with the theoretical prediction. Based on the energy ordering of states in the Franck-Condon regime: at the longest wavelengths ($\lambda > 285.7$ nm) Φ is small, reflecting the relative strength of the $a^3\Pi_1 \leftarrow X$ transition; excitation at shorter wavelengths ($\lambda < 232.6$ nm) results also in low branching fractions, signifying the prevalence of the $A^1\Pi_1 \leftarrow X$ transition; however within the intermediate wavelength range ($\lambda = 263.2$–243.9 nm), I* photofragments are formed in excess of ground state iodine atom I, implying a dominance in this region of the $a^3\Pi_0{}^+ \leftarrow X$ transition. It also can be seen that the theoretical and experimental results coincide in terms of the gross shape and full-width at half maximum of the distribution within their quoted uncertainties, but the peak value of theoretical is slightly greater. As expected, the branching fraction has a maximum about 0.54, and is consistent with the majority of cited corollaries [13–20]. In addition, in the low energy region (34700–36600 cm^{-1}) and in the range of 40000–45000 cm^{-1}, the computation seems to match the ones of Manzhos and Langford et al. [19,20].

As is well known, single photon absorption causes just a change of electronic state of the molecule and it is assumed due to Franck-Condon rule that there is no change in the geometry of the system. Then the system can propagate on the surface of the given state to its minimum or to meet another state, singlet or triplet. Then the system can nonadiabatically transfer from one state to another if there is a crossing between them. In the former case the internal conversion can take place, the intersystem crossing takes place in the latter case. In the case of crossing of two surfaces of two states of the same symmetry a conical intersection (or an avoided crossing) can occur. Under the adiabatic description of the fragmentation mechanism, the asymptotic product channel with which the PES correlates is determined once the nature of the PESs that initially populated is established. Therefore, the quantum yield Φ for H + I* following photolysis of HI at wavelengths in the A band regime should be consistent with the expected behavior of the energy dependence of the partial extinction intensities for transitions $A^1\Pi_1$, $a^3\Pi_1$ and $a^3\Pi_{0+} \leftarrow X$. Thus, one possible reason for the deviation from the experimental Φ values may be the ignorance of the necessary perpendicular contribution arising from the constructive interference at the extended bond lengths between the translational wavefunction associated with the initially populated state of 1_u symmetry such as

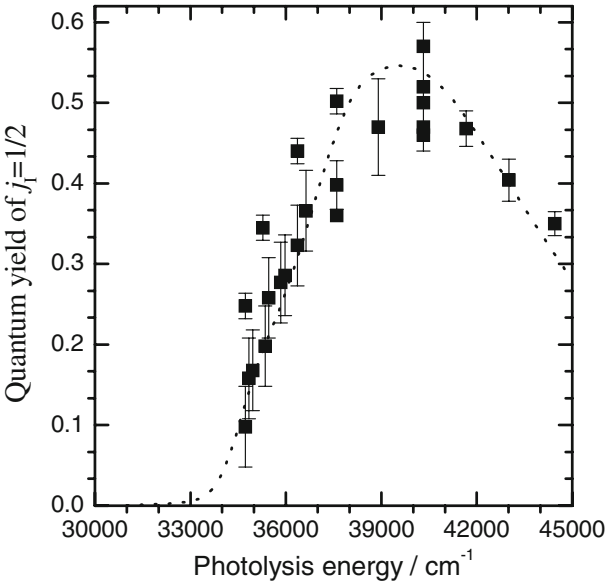

Fig. 4 The calculated I* quantum yield (*dotted line*) in comparison with experimental results in photodissociation of HI: *filled squares with error bars* (Refs. [13–20])

$A^1\Pi_1$ state, from which the subsequent nonadiabatic coupling to other $\Omega = 1$ states nearby the crossing region, and where the exchange interaction is not important. To conclude, many parameters and details can have impacts on the wavelength dependence of quantum yield. Therefore, theoretical agreement versus the near quantitative experiment is seen to be acceptable and reasonable from the methodological standpoints, indicating that the predictions via the simulated spectrum are encouraging in general. The results also suggest that the probability of intersystem crossing can be neglected.

4 Conclusions

The photofragmentation of hydrogen iodide is examined by performing electronic structure calculations and simulation techniques. The extinction cross-sections and final product state population are obtained by the numerical calculations, which exhibit a good agreement with the previous experimental results. The electronic transitions are investigated by employing the time-dependent density functional theory, which along with the quantum yield calculations reproduce the experimental results accurately. The results also suggest that the probability of intersystem crossing in the photodissociation of HI can be neglected.

References

1. G.E. Hall, P.L. Houston, Annu. Rev. Phys. Chem. **40**, 375 (1989)

2. H. Dietz , V. Engel, Chem. Phys. Lett. **255**, 258 (1996)
3. M.S. Child, R.B. Bernstein, J. Chem. Phys. **59**, 5916 (1973)
4. N. Gador, H.O. Karlsson, T. Hansson, Phys. Rev. A **70**, 033418 (2004)
5. A.S. Bracker, E.R. Wouters, A.G. Suits, O.S. Vasyutinskii, J. Chem. Phys. **110**, 6749 (1999)
6. A.J. Alexander, Z.H. Kim, S.A. Kandel, R.N. Zare, T.P. Rakitzis, Y. Asano, S. Yabushita, J. Chem. Phys. **113**, 9022 (2000)
7. M.J. Bass, M. Brouard, A.P. Clark, C. Vallance, B. Martinez-Haya, Phys. Chem. Chem. Phys. **5**, 856 (2003)
8. T.P. Rakitzis, T.N. Kitsopoulos, J. Chem. Phys. **116**, 9228 (2002)
9. M.N.R. Ashfold, J.E. Baggott, *Molecular Photodissociation Dynamics* (Royal Society of Chemistry, London, 1987)
10. J.P. Simons, J. Phys. Chem. **88**, 1287 (1984)
11. M.J. Molina, F.S. Rowland, Nature **249**, 810 (1974)
12. M.J. Molina, F.S. Rowland, J. Phys. Chem. **79**, 667 (1975)
13. R.D. Clear, S.J. Riley, K.R. Wilson, J. Chem. Phys. **63**, 1340 (1975)
14. R. Schmiedl, H. Dugan, W. Meier, K.H. Welge, Z. Phys. A **304**, 137 (1982)
15. P.M. Regan, D. Ascenzi, C. Clementi, M.N.R. Ashfold, A.J. Orr-Ewing, Chem. Phys. Lett. **315**, 187 (1999)
16. I. Levy, M. Shapiro, J. Chem. Phys. **89**, 2900 (1988)
17. G.N.A. van Veen, K.A. Mohamed, T. Baller, A.E. de Vries, Chem. Phys. **80**, 113 (1983)
18. E.C.Y. Inn, J. Atmos. Sci. **32**, 2375 (1975)
19. S.R. Langford, P.M. Regan, A.J. Orr-Ewing, M.N.R. Ashfold, Chem. Phys. **231**, 245 (1998)
20. S. Manzhos, H.P. Loock, B.L.G. Bakker, D.H. Parker, J. Chem. Phys. **117**, 9347 (2002)
21. K. Andersson, M.P. Fulscher, R. Lindh, P.-Å. Malmqvist, J. Olsen, A.J. Sadlej, P.-O. Widmark, *MOLCAS, version 5.4* (University of Lund, Lund, Sweden, 2000)
22. Z. Barandiaran, L. Sijo, Can. J. Chem. **70**, 409 (1992)
23. R.J. LeRoy, G.T. Kraemer, S. Manzhos, J. Chem. Phys. **117**, 9353 (2002)
24. K.P. Huber, G. Herzberg, *Molecular Spectra and Molecular Structure*, vol. 4 (Van Nostrand Reinhold, Princeton, 1979)
25. C.C. Marston, G.G. Balint-Kurti, J. Chem. Phys. **91**, 3571 (1989)
26. J.F. Ogilvie, Trans. Faraday Soc. **67**, 2205 (1971)